Original Research Article Analytical Chemistry

International Journal of Pharma and Bio Sciences

ISSN 0975-6299

STRUCTURAL INVESTIGATION AND MODELLING INSIGHT OF 2-BUTOXY-*N*-[2-(DIETHYLAMINO)ETHYL] QUINOLINE-4-CARBOXAMIDE

J. DEVA ANBAN[*1, 3], SAYANTAN PRADHAN[2] AND C. JAMES[3]

[1] Department of Physics, Pioneer Kumaraswamy College, Nagercoil,Tamil Nadu.
[2]Department of Chemistry, Jadavpur University, Kolkata,West Bengal.
[3]Department of Physics and Research Centre, Scott Christian College (Autonomous), Nagercoil, Tamil Nadu.

ABSTRACT

In this study, the anesthetic compound 2-Butoxy-*N*-[2-(diethylamino) ethyl] quinoline-4-carboxamide (BDQ) was optimized with Density Functional Theory (DFT) calculations using B3LYP /6-311+G (d, p) basis set. FT-IR, FT-Raman and UV-visible spectra have been recorded and theoretical calculations were carried out with the aid of Normal Coordinate Analysis (NCA). Hyperconjugative interactions, revealed the stability of the molecule by Natural Bond Orbital (NBO) analysis. The presence of secondary amide increases the stability of the molecule. The biological significance of the molecule is enhanced by the π→π* interactions. Molecular docking studies were carried out to understand the binding of the molecule with the human voltage-gated sodium channels.

KEYWORDS: **DFT, NBO, Cyclic Voltammetry, Molecular docking.**

J. DEVA ANBAN*
Department of Physics, Pioneer Kumaraswamy College, Nagercoil,Tamil Nadu.
Department of Physics and Research Centre, Scott Christian College (Autonomous), Nagercoil, Tamil Nadu.

Received on: 03-04-2017
Revised and Accepted on: 08-05-2017
DOI: http://dx.doi.org/10.22376/ijpbs.2017.8.3.p16-26

INTRODUCTION

Quinoline derivatives play an important role in medicinal chemistry due to their chemical and biological properties. It is used as antimalarial, antibacterial, antifungal, anticancer, antifilarial, anti-amoebic, antiviral, anti-parasitic and anti- tubercular activities.[1-5] Other than this; certain quinoline-based compounds are also used in local pain management as local anesthetics. 2-Butoxy-*N*-[2-(diethylamino) ethyl] quinoline-4-carboxamide (BDQ) is a member of the amide class, long-acting local anaesthetic. It comprises a hydrophobic quinolone ring, a hydrophilic tertiary amine and an intermediate amide linkage. The uncharged local anaesthetic BDQ is more poisonous and the system at the molecular level is still uncertain.[6] Many experimental and theoretical studies of quionline have been investigated but, there are no comprehensive analysis performed on the BDQ molecule so far.[7, 8] This makes us to choose BDQ as targeted molecule. So in the present probe, an attempt has been made to determine the electrophysical and chemical properties of BDQ, which attributes the chemical behaviour of the molecule.

MATERIAL AND COMPUTATION

White crystalline powder of BDQ (spectroscopic grade) was purchased from Sigma-Aldrich Chemicals, USA. The room temperature FT-IR spectrum was recorded in Perkin Elmer Spectrum one instrument with the spectral resolution of 1 cm^{-1} in KBr tablet in the spectral range 4000-450 cm^{-1}. The FT-Raman spectrum was recorded using Brucker: RFS 27 Standalone instrument. The 1064 nm line of Nd:YAG laser source of about 100 mW was used for excitation in the spectral range 4000-50 cm^{-1}. Electrochemical measurements were performed using a home-made two-compartment three-electrode electrochemical cell. A glassy carbon (GC), a Pt wire and a non-aqueous Ag/Ag^{+} were used as working, auxiliary and reference electrodes. Cyclic voltammograms were recorded using CHI638 (CH Instruments, US, Austin) electrochemical analyser. The DFT computation of BDQ was performed using Gaussian 09 program with B3LYP /6-311 +G (d, p) basis set.[9] The harmonic vibrational wave numbers were calculated by normal coordinate analysis (NCA) using MOLVIB program version 7.0.[10] Scaling of the force field was done according to the Scaled Quantum Mechanical Force Field (SQMFF) calculations. NBO analysis was carried out using NBO 3.1.[11] Molecular docking simulations were achieved with AutoDock Vina software.[12] The 3D crystal structure of human voltage-gated sodium channels were acquired from the Protein Data Bank (PDBID: 5EKO). AutoDock Tools (ADT) graphical user interface were used to calculate Kollman charges and to add polar hydrogen.[13]

RESULTS AND DISCUSSION

OPTIMISED GEOMETRY

The optimised molecular structure of BDQ at the DFT/B3LYP-6311+G (d, p) level is shown in Fig.1.Geometrical parameters related to this study are listed in Table1.

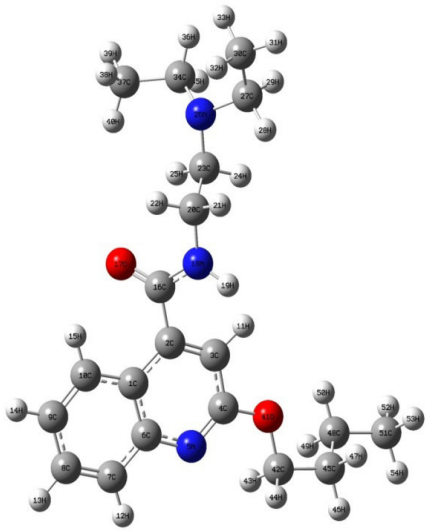

Figure 1
Optimized molecular structure of BDQ

The C-H bond length of the quinoline ring varies through (1.084Å-1.085Å), which is marginally larger than the noticed XRD values (0.95Å) determined crystallographically by Van Eerdenbrugh et al.[14] The increased bond length of C_6-C_7 (1.416Å) when compared to C_7-C_8 (1.378Å) is due to the presence of the adjoining quinolone ring. The C-N distances of C_6-N_5 (1.371Å) and C_{16}-N_{18} (1.364Å) reveal the partial double bond character. The carbon - nitrogen bond distances are found to be much shorter than the average value for a C-N bond (1.47Å), but considerably longer than a C=N (1.22Å), shows some multiple bond character.[15] The asymmetry of bond angles at C_{16} position, C_2-C_{16}-N_{18} (114.8º), C_2-C_{16}-O_{17}

(122.7º), N_{18}-C_{16}-O_{17} (122.3º) indicates the weakening of N_{18}-H_{19}. The existence of an intramolecular C-H…O hydrogen bonding interaction is revealed by the contact H_{15}…O_{17} (2.328Å), which is considerably shorter than the van der Waals separation (2.72 Å).[16]

Table 1
Selected geometrical parameters of BDQ

Parameters	EXPT.	CALC.	DIFF.
Bond length (Å)			
C_3-H_{11}	0.949	1.084	-0.134
C_7-H_{12}	0.950	1.084	-0.134
C_8-H_{13}	0.950	1.084	-0.134
C_9-H_{14}	0.950	1.085	-0.135
C_{10}-H_{15}	0.950	1.085	-0.135
C_{16}-O_{17}	1.235	1.228	0.007
C_6-C_7	1.408	1.416	-0.008
C_7-C_8	1.364	1.378	-0.014
C_1-C_2	1.444	1.436	0.008
C_2-C_3	1.354	1.373	-0.019
C_3-C_4	1.414	1.425	-0.011
C_6-C_7	1.408	1.416	-0.008
C_6-C_1	1.417	1.431	-0.014
C_4-N_5	1.304	1.307	-0.003
N_5-C_6	1.365	1.371	-0.005
C_8-C_9	1.404	1.412	-0.008
C_9-C_{10}	1.368	1.379	-0.011
C_{16}-N_{18}	1.352	1.364	-0.012
BondAngle (˚)			
N_{18}-C_{16}-C_2	115.05	114.80	0.25
O_{17}-C_{16}-C_2	123.46	122.79	0.67
O_{17}-C_{16}-N_{18}	121.44	122.39	-0.95
N_5-C_6-C_1	123.65	123.05	0.60
Dihedral angle (˚)			
C_6-N_5-C_4-O_{41}	-176.46	-179.41	2.95
C_{16}-C_2-C_3-C_4	-176.33	-178.94	2.61
C_1-C_2-C_{16}-N_{18}	142.41	138.24	4.17
N_{18}-C_{20}-C_{23}-N_{26}	-174.51	-179.60	5.09
C_{20}-N_{18}-C_{16}-C_2	177.21	178.51	-1.30
C_{20}-N_{18}-C_{16}-O_{17}	-0.834	-0.15	-0.68

Table 2
Second order perturbation theory analysis of Fock matrix in NBO basis.

Donor (i)	ED (i) (e)	Energy	Acceptor (j)	ED (j) (e)	Energy	E (2) (kcal mol^{-1})
πC_1-C_6	1.5418	-0.2358	π*C_2 -C_3	0.2460	0.0330	19.34
πC_1-C_6	1.5418	-0.2358	π*C_4-N_5	0.3665	0.0166	12.85
πC_1-C_6	1.5418	-0.2358	π*C_7-C_8	0.2594	0.0485	14.85
πC_1-C_6	1.5418	-0.2358	π*C_9-C_{10}	0.2559	0.0504	17.44
πC_2-C_3	1.7637	-0.2698	π*C_1-C_6	0.4502	0.0346	11.81
πC_2-C_3	1.7637	-0.2698	π*C_2-C_5	0.3665	0.0166	22.80
πC_2-C_3	1.7637	-0.2698	π*C_{16}-O_{17}	0.2938	0.0534	11.72
πC_4-N_5	1.7957	-0.3097	π*C_1-C_6	0.4502	0.0346	19.86
σN_5-C_6	1.9778	-0.7890	σ*C_4-O_{41}	0.0499	0.3942	5.33
πC_4-N_5	1.7957	-0.3097	π*C_2-C_3	0.2460	0.0330	9.27
πC_7-C_8	1.7257	-0.2448	π*C_1-C_6	0.4502	0.0346	18.56
σC_7-H_{12}	1.9804	-0.5073	σ*C_4-O_{41}	0.0400	0.5396	4.38
πC_7-C_8	1.7257	-0.2448	π*C_9-C_{10}	0.2559	0.0504	16.75
σC_8-H_{13}	1.9827	-0.5139	σ*C_6-C_7	0.0239	0.5580	4.04
πC_9-C_{10}	1.7220	-0.2423	π*C_1-C_6	0.4502	0.0346	16.38
πC_9-C_{10}	1.7220	-0.2423	π*C_7-C_8	0.2594	0.0485	18.81
σC_{10}-H_{15}	1.9798	-0.5052	σ*C_1-C_6	0.0400	0.5396	4.38
σN_{18}-H_{19}	1.9864	-0.6665	σ*C_{16}-O_{17}	0.0292	0.5509	4.12

LP(2)O_{17}	1.8625	-0.2392	σ*C_{16}-N_{18}	0.0735	0.4792	24.58
LP(2)O_{17}	1.8625	-0.2392	σ*C_2-C_{16}	0.0688	0.4153	20.32
LP(1)N_{18}	1.6956	-0.2535	π*C_{16}-O_{17}	0.2938	0.0534	54.28
LP(1)N_{26}	1.8858	-0.2593	σ*C_{23}-H_{24}	0.0302	0.4365	6.50
LP(1)N_{26}	1.8858	-0.2593	σ*C_{27}-H_{29}	0.0324	0.4394	7.21
LP(1)N_{26}	1.8858	-0.2593	σ*C_{34}-H_{35}	0.0309	0.4443	7.02
LP(1)$_{O41}$	1.9630	-0.5464	σ*C_4-N_5	0.0251	0.5822	7.37
LP(2)$_{O41}$	1.8169	-0.3084	π*C_4-N_5	0.3665	0.0166	39.70
π*C $_1$-C_6	0.4502	0.0346	π*C_7-C_8	0.2594	0.0485	201.74
π*C_1-C_6	0.4502	0.0346	π*C_9-C_{10}	0.2559	0.0504	170.01
π*C_2-C_3	0.2460	0.0330	π*C_{16}-O_{17}	0.2938	0.0534	68.09
π*C_4-N_5	0.3665	0.0166	π*C_1-C_6	0.4502	0.0346	147.35
π*C_4-N_5	0.3665	0.0166	π*C_2-C_3	0.2460	0.0330	153.62

NBO ANALYSIS

Natural bond orbital analysis is a systematic method for finding the intra and intermolecular interactions in a molecule. The intra molecular hyperconjugative interaction in BDQ is formed by the orbital overlap between the π (C_1-C_6) → π*(C_2-C_3), π*(C_4-N_5), π*(C_7-C_8), π*(C_9-C_{10}) with stabilization energies of 19.34, 12.85, 14.85 and 17.44 kcal/mol respectively. From Table2, it is observed that π (C_1-C_6), π (C_2-C_3), π (C_4-N_5) bonding orbitals donate its π electrons to antibonding π*(C_7-C_8), π*(C_{16}-O_{17}) and π*(C_1-C_6) orbitals, with stabilisation energies of 14.85, 11.72 and 19.86 kcal/mol respectively. These orbitals π*(C_1-C_6), π*(C_2-C_3), π*(C_4-N_5) further conjugates with π*(C_7-C_8), π*(C_{16}-O_{17}) and π*(C_1-C_6) antibonding orbitals with immense stabilization energies of 201.74, 68.09 and 147.35 kcal/mol. Lone Pair interactions, LP (2) O_{17} →σ*(C_{16}-N_{18}) and LP (2) O_{17} →σ*(C_2-C_{16}) with energies (24.58, 20.32 kcal/mol) justifies that the resonance of the ring is increased by the electron donating nitrogen atom (N_{18}). This is further validated by the shortening of C_{16}-N_{18} (1.364 Å) and C_{16}-O_{17} (1.228 Å) bonds. The Conjugation between LP (N_{18}) →π*(C_{16}-O_{17}) with energy (54.28 kcal/mol) contribute to the distinct physical and chemical properties of the title molecule. The C_4-N_5 bond is weakened due to the hyper- conjugative interaction of LP (1) O_{41}→σ (C_4-N_5) with a stabilization energy of 7.37 kcal/mol. The bioactivity in the molecule is persuaded by these Intramolecular charge transfers (ICT).

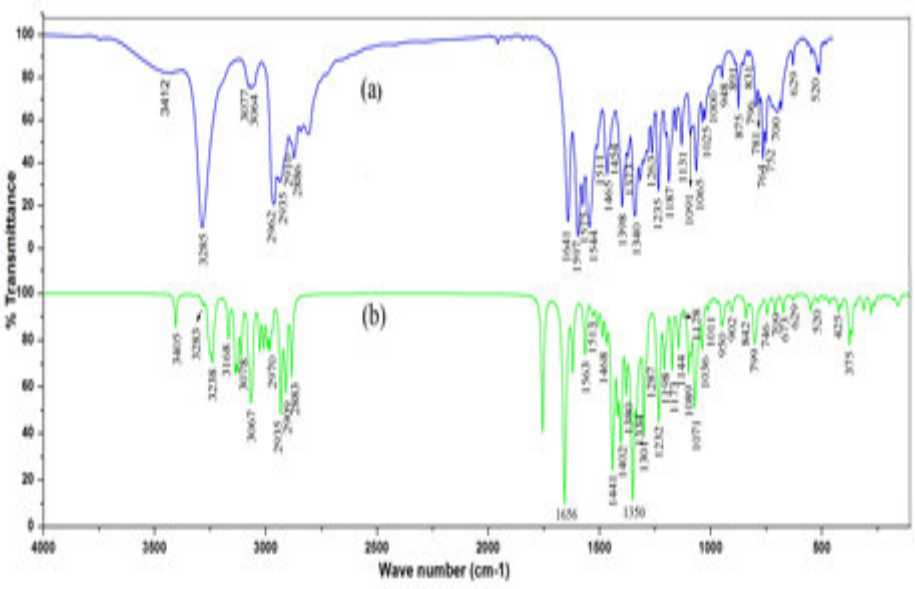

Figure 2
Comparison of (a) experimental and (b) simulated FT-IR spectra of BDQ

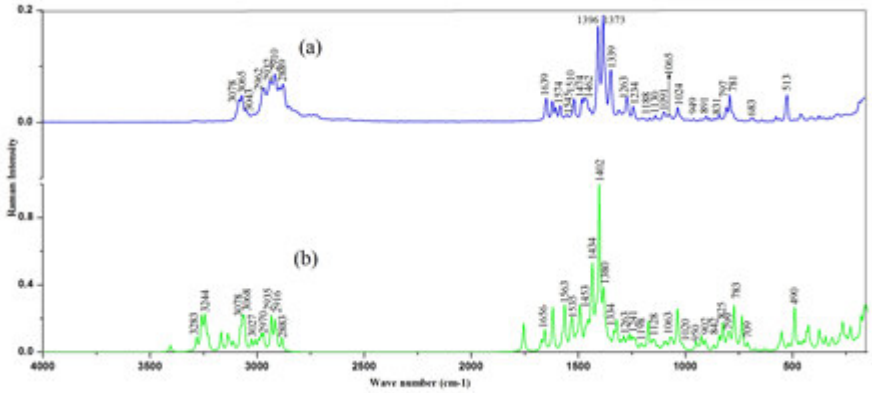

Figure 3
Comparison of (a) experimental and (b) simulated FT-Raman spectra of BDQ

Table 3
Selected vibrational assignments by normal coordinate analysis based on SQM force field calculations

Calculated (DFT)			Observed (cm^{-1})		Assignment
Scaled (cm^{-1})	IR Intensities	Raman Intensities	FT-IR	FT-Raman	
3405	22.14	3.91	3412	-	υNH(100)
2970	15.01	11.7	2965	2962	υCH_{3op}(80),υCH_{3ip}(19)
2935	27.23	21.0	2935	-	υCH_2(98)
2909	65.98	12.9	-	2910	υCH_2(92)
2883	59.21	8.73	2873	2872	υCH_3(96)
1656	332.02	13.4	1641	1639	Q_{asyd}(32),υCO (30), υCC(18)
1563	30.16	28.5	1574	1563	γCC(33), Q_{asyd}(29),Q_{trid}(19)
1535	5.49	17.9	1544	1545	δNH(57),υCC(23),
1513	5.82	10.0	1511	1510	υCN(48), υCC(26)
1468	22.46	14.9	1465	1474	υCC(30), δCC(19)
1453	0.95	19.5	1454	1462	βCH_{3op}(47),βCH_{3ip}(31)
1368	14.52	15.0	1373	1373	τCH_2 (23), ωCH_2(29),
1334	78.48	12.7	1340	1339	υCO(46), υCC(12)
1263	1.49	11.1	1263	1263	CH_{2sci}(28),ρCH_2(16), Q_{trid}(14)
1241	42.33	8.55	1235	1234	δNH(47), υCC(31)
1198	19.64	4.53	1187	1188	δCH(50), δCC(44)
1128	4.60	4.15	1131	1130	υCC(33), δCH(12)
1089	25.44	6.34	1088	1091	υCN(40),ρCH_2(22)
1063	34.54	8.64	1065	1065	δCH(71)
1020	0.28	5.87	1025	1024	δCH(61), υCC(15)
1011	7.49	4.54	1000	-	ρCH_3(27), υCC (19), υCN(11)
950	17.78	6.47	948	949	γCH(59), Q_{asyd}(34)
902	8.31	5.06	891	891	Q_{trid}(51), γCH(25)
842	14.77	10.1	852	851	γCH(61)
825	2.22	17.7	831	831	ωNH(66)
799	19.73	12.1	796	797	Q_{asyd}(66), γCH(23)
783	3.31	8.95	781	781	γCH(32), βCH_{3ip}(27),Q_{asyd}(12)
746	11.64	7.12	752	-	γCH(61), Q_{asydo}(17)
709	4.74	5.76	700	-	γCO (67), Q_{asydo}(14), Q_{asyd} (11)

υ- stretching; β-bending; δ-in-plane deformation; γ -out-of-plane deformation; τ-torsion; ρ- rocking; ω-wagging ;Q -Ring.

VIBRATIONAL ANALYSIS

The experimental and simulated FT-IR and FT-Raman spectra of the title molecule are presented in Fig 2 and 3. Hand-picked spectral assignments along with the calculated FT-IR and FT-Raman intensities pertinent to this study are given in Table 3. In amides the conjugation between the nitrogen LP electrons and the carbonyl π bond results in distinct physical and chemical properties. The secondary amide have only one NH stretching band and that appear in the range 3500-3300 cm^{-1}.[17,18] The NH stretching mode emerges at 3412 cm^{-1} in the FT-IR spectrum and this shifting confirms the existence of an intermolecular N-H…O hydrogen bonding. The C=O stretching band is the characteristic secondary amide band that usually occurs in the region 1680-1630 cm^{-1}. In BDQ, the C=O stretching vibrations are recorded at 1641 cm^{-1} in FT-IR spectrum and 1639 cm^{-1} in FT-Raman spectrum. The lowering of C=O mode is because of the conjugation between the carbonyl

group and the amide nitrogen. This is clearly observed in the geometry as the bond C_{16}-O_{17} lengthens from the values revealed earlier.[19] Also the resulting stabilization energy (54.28 kcal/mol) from the interaction of LP (N_{18}) $\rightarrow\pi^*$ (C_{16}-O_{17}) reveals the degree of conjugation between the nitrogen LP electron and the carbonyl π bond. In mono-substituted amides the CNH vibration, where the nitrogen and hydrogen atoms move in opposite directions relative to the carbon atom absorbs near 1550 cm^{-1},whereas it is nearby 1250 cm^{-1} when the atoms move unvaryingly relative to the carbon atom.[20] These CNH bending modes are observed at 1544, 1235cm^{-1} in FT-IR spectrum and 1545, 1234cm^{-1} in FT-Raman spectrum. The C=C stretching mode of the quinoline ring is observed at 1575 cm^{-1} in FT-IR spectrum and 1574 cm^{-1} in FT-Raman spectrum. The band at 1511cm^{-1} in FT-IR spectrum and 1510 cm^{-1} in FT-Raman spectrum are assigned to C=N stretching mode. The band at 1340 cm^{-1} in FT-IR spectrum and 1339 cm^{-1} in FT-Raman spectrum are assigned to C-N stretching. The band at 1465 cm^{-1}in FT-IR spectrum and 1474 cm^{-1} in FT-Raman spectrum are characterized to C-C stretching. The CH stretching occurs above 3000 cm^{-1} and is typically manifested as multiplicity of weak to moderate bands. All the CH stretching bands are perceived to be weak because of a decrease in the dipole moment (μ= 1.22 Debye). The CH out- of- plane deformations of the ring are observed at 948,891,852,796,781,752 cm^{-1} in the FT-IR spectrum and 949,891,851,797,781 cm^{-1} in the FT-Raman spectrum. The CH in- plane deformation bands are predicted above 1000 cm^{-1}. In the present case, these bands are glimpsed at 1187, 1131, 1065, 1025cm^{-1} in the FT-IR spectrum and 1188, 1130, 1065, 1024 cm^{-1} in the FT-Raman spectrum. The titled molecule possesses three methyl groups which lie in the ultimate of the molecule. The asymmetric stretching vibration is mostly at higher wave number than the symmetric stretching vibration. In the present assignment the symmetric CH stretching mode is observed at 2886 cm^{-1} in FT-IR spectrum and 2889 cm^{-1} in FT-Raman spectrum. The band at 2962 cm^{-1} in FT-IR and FT-Raman spectra are assigned to the CH_3 asymmetric stretching mode. The in-plane bending methyl deformation is observed at 1454 cm^{-1} in FT-IR spectrum and 1462 cm^{-1} in FT-Raman spectrum. The band at 1000 cm^{-1} in FT-IR spectrum is assigned to CH_3 rocking mode. The stretching wavenumbers of methyl groups are not much affected, because the charge redistribution focuses only the amide group. The asymmetric and symmetric methylene stretching vibration is normally occurring in the region 3000 -2800 cm^{-1}. In the present case, the stretching modes are assigned at 2935 and 2910 cm^{-1} in FT-IR spectrum, 2932 and 2910 cm^{-1} in FT-Raman spectrum. The CH_2 wagging mode is observed at 1373 cm^{-1} in FT-IR and FT-Raman spectra. The computed spectra are in accordance with the experiment spectra.

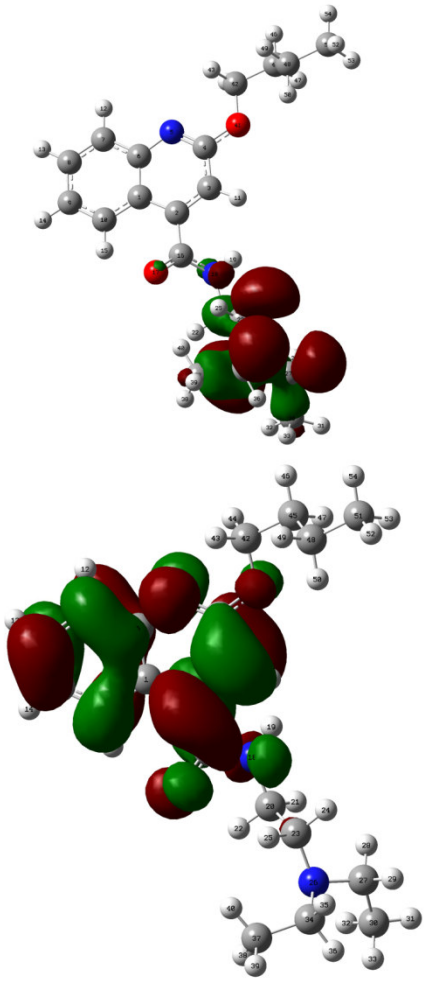

Figure 4
The atomic orbital compositions of the frontier molecular orbitals

FRONTIER MOLECULAR ORBITAL ANALYSIS

The energy gap between the highest occupied molecular orbital (HOMO) and the lowest unoccupied molecular orbital (LUMO) plays a prime role in determining the chemical reactivity, chemical hardness and softness of a molecule. Fig.4 displays the HOMO–LUMO plots of BDQ. The energy gap (E_g) is 4.206 eV, which indicates the high kinetic susceptibility of the molecule. Hard, soft nucleophiles and electrophiles are directly associated with E_{HOMO} and E_{LUMO} orbitals. High value of E_{HOMO} (-5.707 eV) indicates that the BDQ has a tendency to donate more electrons and it behaves as a soft nucleophile. From the plot, it is found that HOMO is largely localised over the diethyl amino group and LUMO is localised on the quinoline ring. This shows the intramolecular charge transfer is taking place from the diethyl amino group.

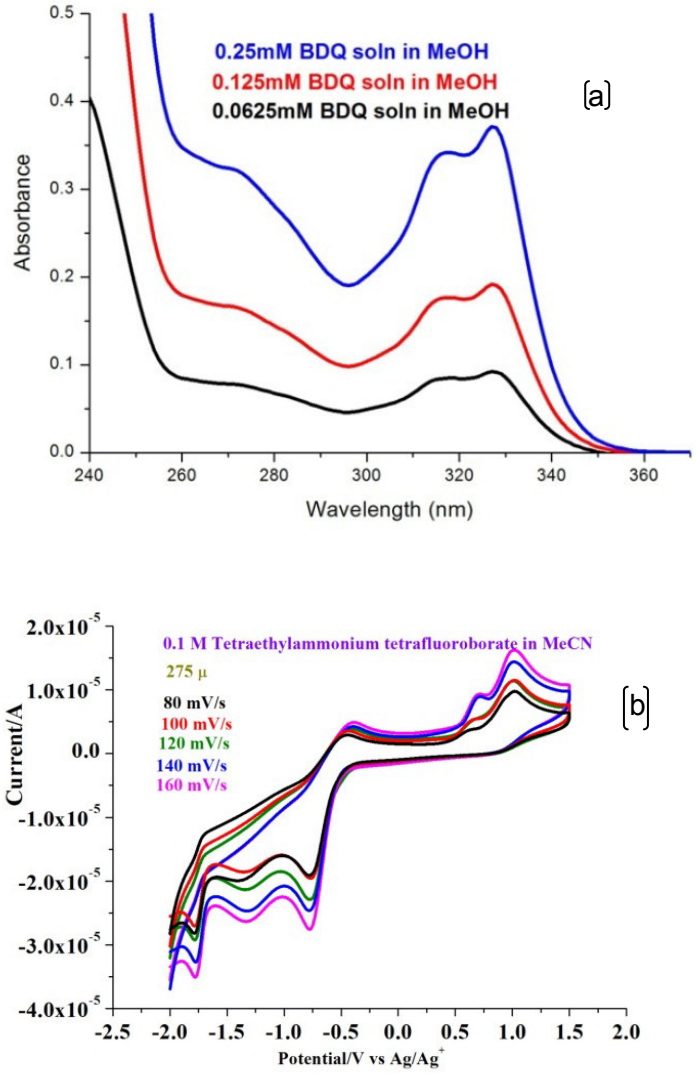

Figure 5

(a) Absorption spectra of BDQ at various concentrations

(b) Cyclic voltammogram at different scan rates

UV-VIS ABSORPTION SPECTRA

Calculation of UV–Vis absorption spectrum was done with the TD-DFT method using B3LYP- 6-311+ G (d, p). The experimental UV-Vis spectrum of the title compound in methanol was recorded and is exhibited in Fig.5 (a). Quantum chemical calculations show electronic transitions are observed at 344 and 310 nm, which is in accordance with the experimental values at 327 and 316 nm. The electronic absorption substantiates the transition between HOMO (93) and LUMO (94). The prolonged absorption wave length is used to calculate the optical band gap energy, E_g according to the equation

$$E_g = \frac{1242}{\lambda_{max}} \text{ eV} \quad \text{.....(1)}$$

where λ_{max} is the wavelength of maximum absorption, which is found to be E_g=3.798 eV.

ELECTROCHEMICAL ANALYSIS

Cyclic voltammetry analysis is performed to determine the oxidation and reduction potentials of the given molecule. It plays a crucial role in correlating the HOMO-LUMO energies, ionisation potential and electron affinity. Fig.5 (b) shows the cyclic voltammogram of BDQ at different scan rates (80, 100,120,140,160 mVs^{-1}) in the -2.0 to +2.0 V potential ranges. The anodic peak current changes linearly with the square root of the sweep rate, and it slightly shifts to more positive side. The oxidation potential is found at 1.02 V and a less prominent reduction wave at -1.99 V. In order to estimate the ionization potential IP and electron affinity EA of the title molecule it is necessary to relate the electrochemical potentials at the vacuum level.[21]

$$IP = (E_{OX} + 4.4)\ eV \quad \text{..... (2)}$$

$$EA = (I_p - E_g)\ eV \quad \text{..... (3)}$$

where E_{OX} is the onset potential of the oxidation wave compared with the reference electrode. The value 4.4 represents the difference between the vacuum level potential of the normal hydrogen electrode and the potential of the Ag electrode. E_{HOMO} is directly proportional to the oxidation potential. The high E_{HOMO} (-5.42 eV) makes the oxidation more difficult, which requires strong potential to oxidise the molecule. The hypothetical E_{HOMO} (-5.707eV) agrees well with the voltammetric result.

Table 4

HOMO-LUMO energy values and related molecular properties

Orbital	eV
E_{HOMO}	-5.707
E_{LUMO}	-1.498
E_g	4.206
Hardness (η)	2.104
Potential (μ)	-3.602
Softness (S)	1.356
Electronegativity (χ)	3.602
Electrophilicity Index (ω)	3.084
Additional Electronic Charge (ΔN_{max})	1.712
Nucleofugality (ΔE_n)	1.585
Electrofugality(ΔE_e)	8.791

GLOBAL REACTIVITY DESCRIPTORS

The global chemical reactivity descriptors, such as hardness (η), chemical potential (μ), softness (S), electronegativity (χ), electrophilicity index (ω), additional electronic charge (ΔN_{max}), nucleofugality (ΔE_n) and electrofugality (ΔE_e) are calculated[22,23] with the help of HOMO–LUMO energy using the following equations (4-11) and are furnished in Table 4.

$$\eta = \frac{(I-A)}{2} \quad \text{..... (4)}$$

$$\mu = -\frac{(I+A)}{2} \quad \text{..... (5)}$$

$$S = \frac{1}{\eta} \quad \text{..... (6)}$$

$$\chi = \frac{(I+A)}{2} \quad \text{..... (7)}$$

$$\omega = \frac{\mu^2}{2\eta} \quad \text{..... (8)}$$

$$\Delta N_{max} = -\frac{\mu}{\eta} \quad \text{..... (9)}$$

$$\Delta E_n = -A + \omega = \frac{(\mu+\eta)^2}{2\eta} \quad \text{..... (10)}$$

$$\Delta E_e = I + \omega = \frac{(\mu-\eta)^2}{2\eta} \quad \text{..... (11)}$$

where, IP= $-E_{HOMO}$ and EA= $-E_{LUMO}$

The small chemical hardness (2.104 eV) reveals BDQ as a soft molecule. This is also validated from the small HOMO-LUMO energy gap (E_g). The minimal energy E_g shows the molecule is more reactive. The computed electrophilicity index (3.084) is a positive quantity and this calculates the stabilisation energy when the system gains an additional electronic charge from the environment. It holds information about both electron transfer and stability, which is a desirable descriptor of global chemical reactivity. The assistance of these parameters helps in understanding the various pollutants in terms of their reactivity and site selectivity.

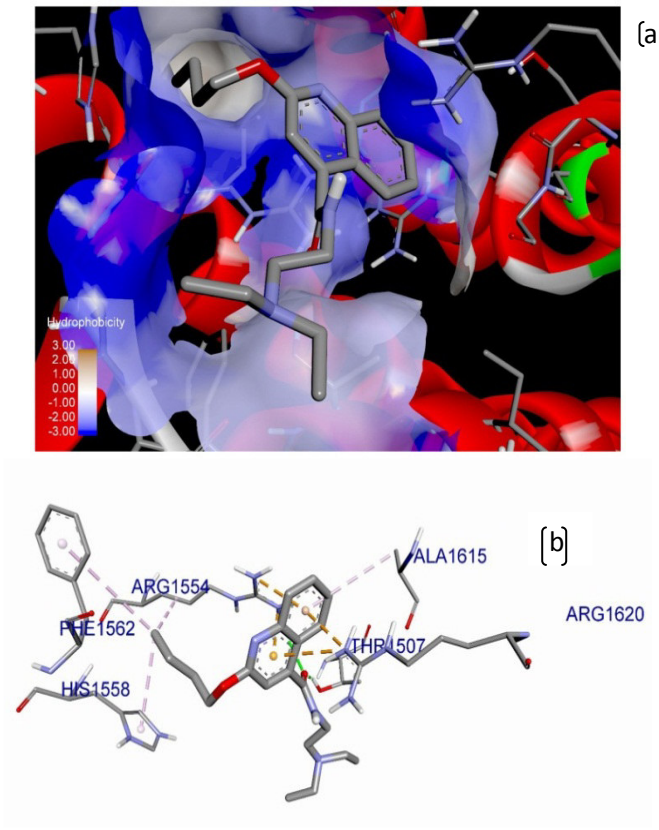

Figure 6
(a) Comprehensive perception of voltage-gated sodium channels and BDQ, (b) Molecular Interactions of ligand with voltage –gated sodium channel amino acids

Table 5
Interaction analysis of docking

Bond Name	Distance (Å)	Bond category	Bond type
A:THR1507:HG1 - :BDQ:O11	2.149	Hydrogen Bond	Conventional Hydrogen Bond
A:ARG1554:HH21 – :BDQ:O11	3.037	Hydrogen Bond	Conventional Hydrogen Bond
A:ARG1554:NH1 – :BDQ	3.439	Electrostatic	Pi-Cation
A:ARG1554:NH2 – :BDQ	3.969	Electrostatic	Pi-Cation
A:ARG1620:NH2 - :BDQ	3.927	Hydrogen Bond; Electrostatic	Pi-Cation; Pi-Donor Hydrogen Bond
A:ARG1620:NH2 - :BDQ	3.234	Electrostatic	Pi-Cation
BDQ:C35 - A:ARG1554	3.420	Hydrophobic	Alkyl
A:HIS1558 - : BDQ:C35	4.188	Hydrophobic	Pi-Alkyl
A:PHE1562 - : BDQ:C35	5.341	Hydrophobic	Pi-Alkyl
:BDQ - A:ALA1615	5.419	Hydrophobic	Pi-Alkyl

MOLECULAR DOCKING ANALYSIS

Molecular docking simulations give information about the binding site and the pharmacological mode of action of drugs. The duration of action of local anaesthetics depends on the protein binding properties.[24] In the present study, the ligand is prepared by minimizing its energy at B3LYP/6-311+G (d, p) level of theory. Active site of the protein is defined in a way that it includes residues within the grid dimensions of 30 X 30 X 30 Å. The most well liked algorithm, Lamarckian Genetic Algorithm (LGA) is used for docking.[25] BDQ targets the voltage-gated sodium channels and binds within the inner pore of the channel.[26] From the docking analysis; it is presumed that hydrophobic interactions and polar contacts collectively constitute the primary force for the binding of the molecule. The ligand that binds to the substrate by hydrophobic interactions is shown in Fig.6 (a). As evident from Table 5, the docked BDQ shows that the residue ALA1615 plays a vital role in this receptor activity by having π- π stacking interaction. ARG1554, HIS1558, PHE1562 are having hydrophobic and THR1507, ARG1554 forms hydrogen bond interactions with the ligand moiety. The interaction of ligands with Nav channel amino acids omitting the Nav channels is depicted in Fig.6 (b). BDQ forms a stable state with human voltage-gated sodium channels, which is evident from its binding affinity of -4.7 kcal.mol^{-1}. From the docking simulation, interaction of BDQ with Nav channel throw light in the binding pattern of anesthetics and how it block both the initiation and conduction of nerve impulses by decreasing the neuronal membrane's permeability by binding in the inner pore of the sodium channel. The BDQ binding site will show the path for the future amide-type local anesthetic drug inventors.

CONCLUSION

2-Butoxy-*N*-[2-(diethylamino) ethyl] quinoline-4-carboxamide and its interactions were studied at the molecular level. The geometrical parameters agree well with the XRD data. Vibrational analysis discloses the existence of an N- H…O intermolecular interaction which is confirmed by the lowering of the carbonyl stretching wave number, which influences the bioactivity of the compound and acts as an active site. The low value of energy gap (E_g) indicates the molecule is more polarizable, which also facilitates the possibility of intramolecular charge transfer. The molecule is associated with high chemical reactivity, low kinetic stability and is termed as a soft molecule. Based on the electrochemical and electronic absorption experiments, parameters such as IP, EA and E_g are quantified to comprehend the electrical and chemical properties of BDQ. From molecular docking studies, it binds to the inner pore and blocks Nav channels in peripheral neurons.

ACKNOWLEDGEMENTS

The author thanks the University Grants Commission (UGC) India, for conferring a Teacher Fellowship under the FDP scheme leading to Ph.D. The author also thanks SAIF, Chennai for the support in recording the FT-IR and FT-Raman spectra.

CONFLICT OF INTEREST

Conflict of interest declared none.

REFERENCES

1. Bilker O, Lindo V, Panico M, Etiene AE, Paxton T, Dell A, Rogers M, Sinden RE, Morris HR. Identification of xanthurenic acid as the putative inducer of malaria development in the mosquito. Nature 1998 Mar 19; 392(6673): 289-92.
2. Fang KC, ChenYL, Sheu JY, WangTC, Tzeng CC. Synthesis, antibacterial and cytotoxic evaluation of Certain 7-substituted norfloxacin derivatives, J. Med. Chem. 2000 Oct 5; 43(20):3809-12.
3. Castelli MV, Kouznetsov VV, , Lopez SN, Sortino M, Enriz RD, Ribas JC, Zacchino S. In vitro antifungal activity of new series of homoallylamines and related compounds with inhibitory properties of the synthesis of fungal cell wall polymers. Bioorg..Med..Chem. 2003 Apr 30 ; 11(7): 1531-50.
4. Dassonneville L, Lansiaux A, Wattelet A, Wattez N, Mahieu C, Van Miert S, Pieters L, Bailly C. Cytotoxicity and cell cycle effects of the plant alkaloids cryptolepine and neocryptolepine: relation to drug-induced apoptosis. Eur. J. Pharmacol. 2000 Dec 1; 409(1): 9-18.
5. Tewari S, Chauhan PMS, Bhaduri DP. Syntheses and antifilarial profile of 7-chloro-4-(substituted amino) quinolines: a new class of antifilarial agents. Bioorg. Med. Chem. Lett. 2000 Jul 3; 10 (13): 1409-12.
6. Daniels TC. Textbook of Organic, Medicinal and Pharmaceutical Chemistry. Wilson CO, Gisvold O, editors. Lipincott: 1962.
7. Nayyar A, Malde A, Coutinho E, Jain R. Synthesis, anti-tuberculosis activity and 3D-QSARstudy of ring-substituted-2/4-quinolinecarbaldehyde derivatives. Bioorg. Med. Chem. 2006 Nov 1; 14 (21): 7302- 10.
8. Manoj E, Kurup MP, Suresh E. Synthesis and Spectral Studies of bisthiocarbohydrazone and biscarbohydrazone of quinoline-2-carbaldehyde: Crystal Structure of bis (quinoline-2- aldehyde) thiocarbohydrazone. J. Chem. Cryst. 2008 Mar 1; 38:157-61.
9. Frisch MJ, Trucks GW, Schlegel HB, Scuseria GE, Robb MA, Cheeseman JR, Scalmani G, Barone V, Mennucci B, Petersson GA, Nakatsuji H. J. Gaussian 09, Revision B. 01, Gaussian. Inc., Wallingford, CT. 2010.
10. Sundius T. Molvib - A flexible program for force field calculation. J. Mol. Struct. 1990 Mar 1; 218; 321–6
11. Glendening ED, Reed AE, Carpenter JE, Weinhold F. NBO Version 3.1, TCI. University of Wisconsin, Madison; 1998.
12. Trott O, Olson AJ. AutoDock Vina: Improving the speed and accuracy of docking with a new scoring function, efficient optimization and multithreading. Journal of Comput. Chemistry. 2010 Jan 30; 31(2): 455-61.
13. BIOVIA DS. Discovery studio modelling environment, San Diego, Dassault Systems, Release 2015;4..
14. Van Eerdenbrugh B, Fanwick PE, Taylor LS. 2-Butoxy-N-[2-(diethylamino) ethyl] - quinoline-4-carboxamide (dibucaine). ActaCryst.E. 2010 Dec 1; 66(12): o3189.
15. Holleman AF, Wiberg N. Inorganic Chemistry, , Academic, New York. 2001.
16. Sato H, , Murakami R, Noda I, Ozaki Y. Infrared and Raman spectroscopy and quantum chemistry calculation studies of C–H···O hydrogen bondings and thermal behavior of biodegradable polyhydroxyalkanoate. J. Mol. Struct. 2005 Jun 3; 744: 35-46.
17. Spire A, Barthes M, Kellouai H, DeNunzio G. Far-infrared spectra of acetanilide revisited. Physica D: Nonlinear Phenomena. 2000 Mar 15; 137(3): 392– 01.
18. Bellamy LJ. The Infrared Spectrum of Complex Molecules. Springer Science & Business Media; 2013 mar 9.
19. Abraham JP, Sajan D, Joe IH, Jayakumar VS. Molecular structure, spectroscopic studies and first-order molecular hyperpolarizabilities of p-amino acetanilide. Spectrochim. Acta A 2008 Nov 15; 71(2): 355-67.
20. Colthup NB. Introduction to Infrared and Raman spectroscopy. Elsevier, 2012 Dec 2. ,

21. Trasatti S. Structuring of the solvent at metal/solution interfaces and components of the electrode potential. J. Electroanal. Chem. 1983 Jul 25; 150(1-2): 1-15.
22. Parr RG, Pearson RG. Absolute hardness: comparison parameter to absolute electronegativity. J Am Chem Soc 1983 Dec 28; 105(26): 7512-16.
23. Koopmans T. Ordering of wave functions and eigen energies to the individual electrons of an atom. Physica 1993; 1(1):104-13.
24. Ebenezer VR, Balakrishnan C, Rajarajan C, Elumalai M. A comparative study of two local anaesthetic agents- Bupivacaine and Lignocaine in dentistry. Int J Pharm Bio Sci 2013 Jan; 4(1): 955 – 9.
25. Gasteiger J, Marsili M. Iterative partial equalization of orbital electronegativity - a rapid access to atomic charges. Tetrahedron 1980 Jan 1; 36(22): 3219-28.
26. Fozzard HA, Sheets MF, Hanck DA. The sodium channel as a target for local anesthetic drugs. Front Pharmacol 2011Nov 1; 2(68): 1-6.

Reviewers of this article

Prof. Srawan Kumar G.Y

Associate Professor,Nalanda Institute of Pharmaceutical Sciences, Sattenapalli, Guntur, Andrapradesh, India

S Mary Delphine M.Sc.,M.Phil,Ph.D

Associate Prof,Dept of Physics,Holy cross college,Nagercoil,India

Prof.Dr.K.Suriaprabha

Asst. Editor , International Journal of Pharma and Bio sciences.

Prof.P.Muthuprasanna

Managing Editor , International Journal of Pharma and Bio sciences.

We sincerely thank the above reviewers for peer reviewing the manuscript